

Development of an Alginate Array Platform to Decouple the Effect of Multiparametric Perturbations on Human Pluripotent Stem Cells During Pancreatic Differentiation

Thomas C. Richardson, Shibin Mathew, Joseph E. Candiello, Saik K. Goh, Prashant N. Kumta, and Ipsita Banerjee*

Human embryonic stem cells (hESC)-derived functional cells hold great promise for regenerative cell therapy. Currently approved strategies for clinical translation requires the isolation of the hESCs-derived cells in materials allowing transfer of reagents but preventing integration with the host. However, hESC fate is known to be sensitive to its local microenvironment, both chemical and physical. Given the complexity of hESC response to environmental parameters, it will be important to evaluate the cell response to multiple combinatorial perturbations. Such complex perturbations are best enabled by exploiting high-throughput screening platforms. In this study, the authors report the effect of multivariate perturbations on hESC differentiation, enabled by the development of high throughput 3D alginate array platform. Specifically, the sensitivity of hESC propagation and pancreatic differentiation to substrate properties and cell culture configuration is analyzed. Cellular response to array perturbations is analyzed by quantitative imaging, and cell sensitivity was determined through statistical modeling. The results indicate that configuration is the stronger determinant of hESC proliferation and differentiation, while substrate properties fine-tune the expression around the average levels. This platform allowed for multiparametric perturbations, and in combination with statistical modeling, allows to identify the sensitivity of hESC proliferation and fate to multiparametric modulation.

1. Introduction

Human pluripotent stem cells (hPSCs) have enormous potential in tissue engineering and cell therapy applications.^[1] These cells have two distinct characteristics which make them

Dr. T. C. Richardson, Dr. S. Mathew, Dr. I. Banerjee
Department of Chemical and Petroleum Engineering
University of Pittsburgh, Pittsburgh, USA
E-mail: ipb1@pitt.edu

Dr. J. E. Candiello, Dr. S. K. Goh
Department of Bioengineering
University of Pittsburgh, Pittsburgh, USA

Dr. P. N. Kumta
Department of Bioengineering, Chemical and Petroleum Engineering,
Mechanical Engineering and Materials Science
University of Pittsburgh, Pittsburgh, USA

DOI: 10.1002/biot.201700099

highly attractive: they can become any cell type in the body, and can self-renew indefinitely. Over the last two decades there has been concentrated effort to derive functional organ specific cells from hPSCs, which include, but are not limited to, cardiac cells,^[2–4] neurons,^[5,6] hepatocytes,^[7–9] and pancreatic beta cells.^[10–13] With the recent success in deriving functional cells from hPSCs, the current emphasis is on translating these cells to the clinic, as a regenerative cell source to replace donor organs. Successful clinical translation of stem cell-derived organs will require a few additional aspects, including i) scalable production of these cells to meet clinical demand and ii) encapsulation in a retrievable device to allow immune protection as well as prevent integration with host.

Encapsulation using biomaterials which form a semi-permeable membrane is a promising strategy for immune protection of implanted cells. Pancreatic islets encapsulated in alginate capsules have been shown to successfully support islet viability and function upon transplantation.^[14–16] More recently, we have

adopted encapsulation for the production of stem cell-derived pancreatic cells.^[17] Furthermore, encapsulation allows culture of cells in 3D, which, in combination with bioreactors, can satisfy scalable cultures to achieve translation potential.^[18] Hence encapsulation is emerging as a promising avenue to meet both biomufacturing goals and immune protection/isolation in a single platform. However, the stem cell fate being highly sensitive to its local microenvironment will likely be modified by the properties of the encapsulating material. Such microenvironments can constitute soluble chemicals/growth factors, interactions with the extracellular matrix (ECM) proteins, cell–cell contact, or physical stimuli such as stiffness or tension. In 2006, Engler et al. showed that culture of mesenchymal stem cells (MSC) on substrates of stiffness's matching those of tissues in the body, resulted in tissue stiffness specific differentiation of the MSCs.^[19] In our earlier published work, we demonstrated the effect of substrate properties using fibrin and alginate, on the differentiation of

mouse embryonic stem cells (mESCs).^[20,21] More recently, we demonstrated the feasibility of pancreatic differentiation of hESCs within alginate capsules^[17]; and identified the range of alginate capsule properties supportive of pancreatic maturation.^[22] Another important insoluble cue which can influence hPSC differentiation is cell–cell contact, especially in 3D cellular aggregates. Lee et al. showed controlling hPSC colony size could control specification to mesoderm (1200 μm in diameter) or endoderm in the presence of soluble differentiation factors, linking cellular organization to hPSC differentiation.^[23] More specific to pancreatic differentiation, Toyoda et al. demonstrated enhancement of pancreatic induction of hPSCs with increasing cell density in adherent (2D) cultures, which was further improved in aggregate culture.^[24] Thus clinical translation of encapsulated hPSCs will require a thorough evaluation of optimum parameters supporting hPSC growth and differentiation.^[25–27]

In this study, we evaluated the sensitivity of encapsulated hPSCs to multiple combinatorial perturbations. Such combinatorial perturbations are best enabled by employing high throughput screening platforms, which enhances experimental output while minimizing the cost of materials, time of experimentation, and physical space. The sensitivity of stem cells to various environmental factors makes it particularly well suited to be studied using such high throughput platforms. This approach has been used in 2D adherent cultures for screening physical stimuli such as material stiffness,^[28] topography,^[29,30] and extracellular matrix protein or peptide composition,^[31–33] on stem cell attachment, growth, and differentiation. However the complexity of stem cell response limits the information gathered from single perturbations and necessitates combinatorial perturbations. For example, Gobba et al. developed a microengineered hydrogel microarray which can vary substrate stiffness while being functionalized with protein combinations, which was used to test MSC differentiation.^[34] In parallel, the advent of 3D culture of stem cells has initiated the development of array platforms supportive of 3D cell culture. Ranga et al. utilized nanolitre-dispensing technology to synthesize over 1000 unique environments to simultaneously probe the effect of matrix elasticity, degradability, and signaling proteins on mESCs self-renewal and proliferation.^[35] Yang et al. developed a 3D combinatorial ECM hydrogel platform to identify optimal ECM combinations which support lineage specific differentiation of hESCs.^[36] In this study, we developed an alginate array platform to determine the sensitivity of 3D encapsulated hESCs to combinatorial perturbations of the physical microenvironment.

Our objective here is to investigate the effect of alginate properties and encapsulated culture configurations on the propagation and the pancreatic differentiation of hPSCs. The developed alginate array platform allowed for multiparametric perturbations, and quantitative imaging to generate a rich complex dataset. Analysis of the data using a linear statistical model allowed us to decouple the complex interactions between the stem cells and the effect of their microenvironment. Thus, in combination with statistical modeling, the developed platform herein enabled the identification of the sensitivity of stem cell proliferation and pancreatic differentiation to multiparametric modulation.

2. Experimental Section

2.1. Human Embryonic Stem Cell Culture

Undifferentiated (UD) H1 hESCs (WiCell) were maintained on hESC-qualified Matrigel (BD Biosciences) coated tissue culture plastic for 5–7 days in mTeSR1 (StemCell Technologies) at 37 °C and 5% CO₂ before passaging. Experiments were performed with p55-p85 hESCs.

2.2. Alginate Array Formation and hESC Encapsulation

Fabrication of the 3D alginate array was done by adopting an approach developed previously by Fernandez et al.^[37] The 3D alginate array was created by coating the culture surface with nitrocellulose (Fisher), followed by spotting 0.5–5 μl of a BaCl₂-poly-(l-lysine) (PLL) mixture in the desired array configuration using a Eppendorf Repeater Plus pipette. The BaCl₂-PLL spot was dried, after which the alginate solution was added directly to the dried spot, resulting in alginate hydrogel crosslinking and attachment to the culture surface. To vary alginate crosslinking, the barium concentration in the BaCl₂-PLL mixture was varied from 10–500 mM. Although in some cases, increase in cation concentration did not significantly increase the substrate stiffness, a broad range of BaCl₂ was chosen to comprehensively test its effect on pancreatic differentiation and test the sensitivity of differentiation on the matrix properties.

For hESC encapsulation, hESC were treated with 10 μm Y-27632 (R&D Systems, Minneapolis, MIN) for 2 h prior to harvesting by Accutase (Invitrogen) treatment for 5–7 min. For encapsulation of single cells, 3 or 5 $\times 10^6$ cells ml⁻¹ were suspended in 1.1% (w/v) low viscosity alginate (Sigma–Aldrich) with 0.2% (v/v) gelatin (Sigma–Aldrich), and was spotted onto the dried BaCl₂-PLL spots as described above. hESC aggregates were formed by culturing the Y-27632-treated single cell suspension of hESC in low adherence 30 mm dishes on a plate shaker set at 55 rpm, at 37 °C and 5% CO₂. Cells were seeded at 1 $\times 10^6$ cells ml, using 2 ml of media in each 30 ml dish. Aggregate formation was allowed to proceed for 2 days on the plate shaker before collecting and encapsulation the alginate array, as described above. The resulting aggregates were suspended in 1 ml of alginate for encapsulation in the array.

2.3. hESC Differentiation

The stage-wise induction protocol for the pancreatic differentiation of hESCs was identical to our previous study, ending at the pancreatic progenitor stage instead of the maturation stage.^[17] Encapsulated single cells were propagated for 4 days in mTeSR1 with 10 μm Y-27632 followed by 2 days in mTeSR1 alone. Preformed aggregates were allowed to acclimate to the hydrogel for 2 days in mTeSR1 prior to starting differentiation. First, DE was induced using 100 ng ml⁻¹ ActivinA (R&D Systems) with 25 ng ml⁻¹ Wnt3A (R&D Systems) for 4 days. Afterwards, PP was induced with 0.2 μM KAAD-cyclopamine (CYC, Millipore) for 2 days and 0.2 μM CYC with 2 μM retinoic acid (Sigma–Aldrich) for 2 days. All differentiation media was made using

DMEM/F12 (Life Technologies), supplemented with 0.2% BSA and 1xB27[®] (Life Technologies).

2.4. Atomic Force Microscopy

The alginate array was formed as described previously, crosslinked with 10, 50, 150, 200, and 500 mM BaCl₂. AFM force indentation measurements were performed using the MFP-3D Atomic Force Microscope (Asylum Research, CA, USA). The hydrogels were maintained in saline after formation to ensure their hydrated state. The stiffness of each alginate gel was measured at $n = 3$ random locations and approximately 16 force curves were taken over a 4×4 grid at each location on each sample.

2.5. Viability

LIVE/DEAD (Life Technologies) viability assay was performed according to manufacturer's instructions.

2.6. DNA and Protein Immunostaining and Quantification Using LICOR

Encapsulated cells in the alginate array were fixed with 4% formaldehyde for 20 min. Cells were permeabilized with 0.1% Triton-X 100 (Sigma-Aldrich) for 5 min prior to blocking with 10% donkey serum in for 1 h. For primary antibodies, we used goat anti-Ki67 (1:100, Santa Cruz Biotechnology), goat anti-SOX17 (1:400 dilution; R&D Systems), rabbit anti-FOXA2 (1:400 dilution; R&D Systems), goat anti-PDX1 (1:200 dilution; R&D Systems), and rabbit anti-Nkx6.1 (1:400 dilution; R&D Systems). Primary antibody staining was done overnight at 4 °C, followed by the addition of the anti-goat or anti-rabbit IR-conjugated secondary antibody (1:800; LI-COR) for 1 h at room temperature. DNA was stained by addition of Draq5 (1:5000, Fisher) during the secondary antibody step. Encapsulated cells were washed three times with 0.9% saline in between each step of the staining protocol. The entire array was imaged at the same time using Odyssey CLx (LICOR) machine. Protein and DNA expression were quantified using the LI-COR Odyssey and Image Studio software.

2.7. Regression Analysis

To relate the expression of markers representing proliferation and pancreatic differentiation to cation concentration and seeding configuration, linear regression analysis was performed.^[38] In the first stage, the influence of the cation concentration alone was determined using the relation below:

$$\left[\frac{\text{Marker}}{\text{DNA}} \right] = \text{Intercept} + \beta_c C + \beta_{c^2} C^2 + \beta_{c^3} C^3, \quad (1.1)$$

where C denotes the cation concentration. The model parameters, Intercept, and $\beta_{(C)}$'s are estimated by applying the training data on the model and performing optimization to minimize the error between the true response and predicted

response. The process is repeated for each culture configuration and marker separately. A linear least squares error model was selected. The data used for training the model was obtained from the individual experimental repeats using a bootstrapping approach. The technique generates large datasets from a small number of experimental replicates, using sampling with replacement technique.^[39,40] Each such surrogate dataset was selected to contain the same number of cation concentration values (total 5) and configuration types (total 3). The regression analysis was performed on each individual bootstrap dataset and the model parameters and their p values were recorded. The final distribution of the p values and the coefficients was monitored for convergence. Only those models where the R squared values ranged from 0.5 to 0.95 were taken in the final distribution of p values and coefficients and for the current analysis, 1000 such bootstrap datasets were sufficient to make the final conclusions.

To evaluate the relative importance of configuration and cation concentration simultaneously, configuration was added into the equation to get a multiple linear regression model given below:

$$\left[\frac{\text{Marker}}{\text{DNA}} \right] = \text{Intercept} + \sum_{i=1}^3 (\beta_{c_i} C^i) + \sum_{i=2}^3 (\beta_{\text{config}_i} \text{Config}_i) + \sum_{i=2}^3 (\beta_{c \times \text{config}_i} C \times \text{Config}_i). \quad (1.2)$$

In Equation (1.2), the configuration variables are binary. The variables configs 2 and 3 take values of 0/1 or 1/0 or 0/0 simultaneously to represent one configuration at a time. Note that config 1 is chosen as the reference (when configs 2 and 3 are null), and therefore does not explicitly appear as a variable in this equation, but is absorbed by the intercept term. This schema, hence, captures the relative influence of configs 2 and 3 over config 1. Concentration terms occur in two forms, one by itself (third order polynomial) and one as a bi-linear term with configuration. All the coefficients are estimated in a similar manner as discussed above for Equation (1.1), except that the bootstrap data are now sampled to include all the configurations and cation concentrations together for a chosen marker.

3. Results

3.1. 3D Alginate Array Synthesis

The alginate array was constructed by first coating the culture surface with nitrocellulose (Figure 1A), a negatively charged coating. This was followed by depositing a barium (Ba²⁺) chloride-PLL mixture in the desired array configuration (Figure 1B), where positively charged PLL ionically interacts with negatively charged nitrocellulose. Once this coating has dried, the alginate-cell solution was spotted directly on top of the BaCl₂ (Figure 1C). The Ba²⁺ crosslinks the alginate, forming a cell-encapsulating hydrogel, and the PLL serves to ionically adhere the alginate to the nitrocellulose, and thus the culture plate. An example of 5×5 arrays in a well of a 6-well plate can be seen in Figure 1C.

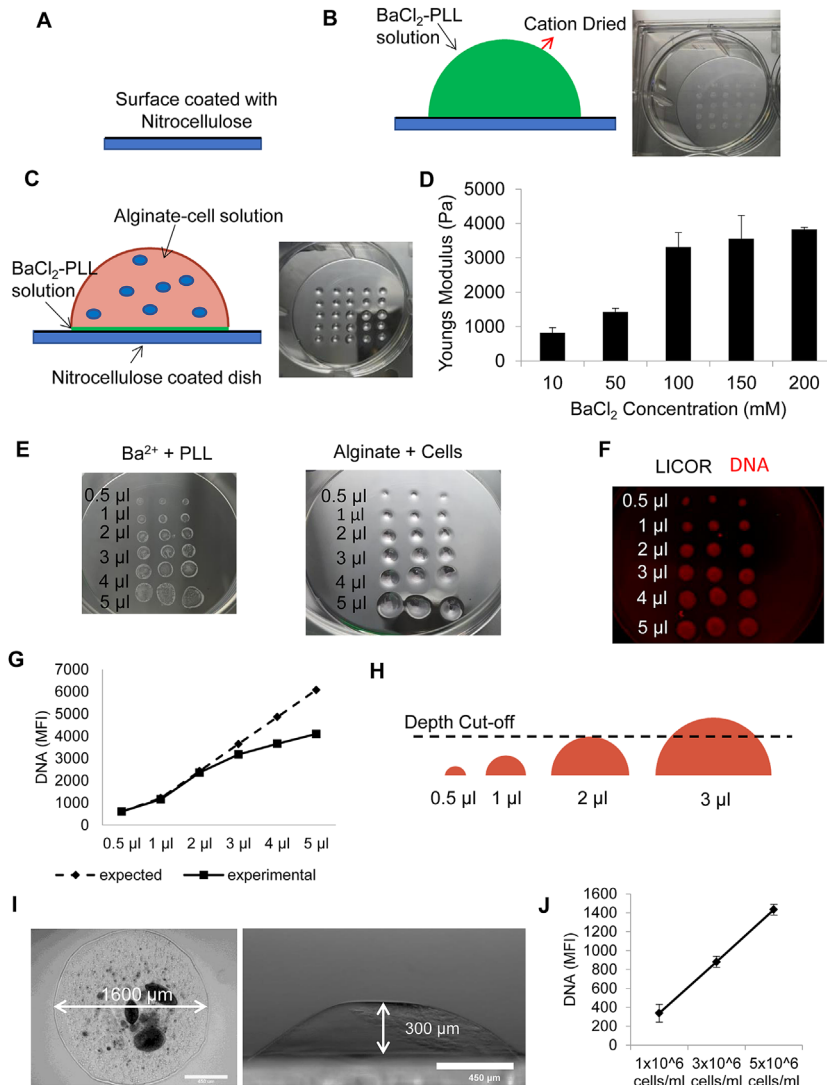


Figure 1. Schematic of 3D alginate array fabrication, array parameter selection and characterization. A) The culture surface is coated with nitrocellulose (black). B) Next, a BaCl₂-poly-(L-lysine) (PLL) mixture is spotted onto the nitrocellulose coated surface in the desired array configuration (green). C) The cell-alginate solution is added directly onto the dried BaCl₂-PLL spot, resulting in crosslinking of the alginate and attachment to the culture surface by ionic interaction between the alginate, PLL, and nitrocellulose. D) The alginate array was formed using 10, 50, 100, 150, 200, and 500 mM BaCl₂ for alginate crosslinking. The resulting alginate hydrogel elastic moduli (Pa) was measured by AFM micro-indentation. E) The array was formed using 0.5, 1, 2, 3, 4, or 5 μl of the cation and alginate solutions. Cells were encapsulated in the array at a density of 1 × 10⁶ cells ml⁻¹. Increase of the cation and alginate volume resulted in correspondingly larger array spots. F) Cell DNA was stained with DraQ5, and imaged using the LICOR Odyssey scanner. G) DNA expression was quantified using the LICOR Image studio software. The dashed line represents the expected MFI if the detection limits are not exceeded due to hydrogel thickness. The solid line is the experimental DNA MFI as the array volumes were increased. H) Schematic of the detection limitations of the LICOR Odyssey scanner in the 3D alginate array system. I) Top-down and side-view bright field images of an individual array spot. J) DNA quantification within the alginate array using the volume of 1 μl, as hESC seeding density is increased.

Conceptually, our platform is similar to the one first introduced by the Dordick group for toxicity and mESC differentiation.^[37,41] However, their platform was primarily designed for soluble chemical signals; while we are focused on insoluble physical

signals. We next evaluated the feasibility of modifying the stiffness of the alginate beads within the array by modulating the BaCl₂ (cation) concentration. Our previous work identified a stiffness range of approximately 3–6 kPa to be ideal for cell growth and pancreatic differentiation.^[22] To encompass this stiffness range, we formed the alginate array with varying barium concentrations within the same array, ranging from 20 to 500 mM Ba²⁺. Measurement of the alginate spot stiffness within the alginate array, using atomic force microscopy (AFM) micro-indentation (Figure 1D), shows that the Young's modulus increased from 819 ± 151 Pa for 10 mM Ba²⁺ to 3821 ± 63 Pa for 200 mM Ba²⁺. Increase in cation concentration corresponded with increased Young's modulus of the alginate spots. This simple platform, thus, allows for the synthesis of alginate spots with varying physical properties within the same array. This will enable a convenient procedure to evaluate cell response, both short and long term, to biophysical stimuli.

3.2. 3D Alginate Array Characterization

A critical component of a high throughput platform for studying cell response is the successful integration of appropriate imaging, analysis, and quantification techniques to measure cell response. Our current objective is the quantitative analysis of viability and phenotype of hESCs encapsulated within the array, primarily using immunostaining. Since this system requires analysis of cell aggregates suspended in an alginate hydrogel, and not adherent cells, the imaging technique requires sufficient penetration into both the hydrogel and cell aggregates. For this purpose we integrated the LICOR Odyssey scanner, which utilizes a near infrared wave length to detect and quantitatively measure the fluorescence intensity in immunostained cell and tissue samples. The LICOR near-infrared fluorophores enhance penetration depth, and dramatically reduce autofluorescence. This system is often used for small animal imaging, and is thus well suited for imaging and analysis of encapsulated cell aggregates.^[42–44] However, we first need to determine the optimal volumes for the array spots to ensure adequate signal intensity from encapsulated cells, without exceeding the detection limits of the LICOR scanner. hESCs were encapsulated in the array at 3 × 10⁶ cells ml⁻¹

using 0.5, 1, 2, 3, 4, and 5 μl of the barium (10 mM)/PLL and alginate solutions (Figure 1E). This resulted in increasingly larger alginate spots, with a corresponding increase in cell number, while retaining the same cell density. Cells within each spot was stained using

DRAQ5, which stains cell DNA and is proportional to cell number, and was quantified using the LI-COR Odyssey and Image Studio software (Figure 1F). Figure 1G shows that an increase in the array volume increased the fluorescent signal. Comparison of the quantified MFI (solid line) with the expected MFI based on cell number (dashed line, Figure 1G), showed a close correspondence between the two up until array volume of 2 μl . Further increase in array volume above 2 μl resulted in a decrease in the measured MFI from the expected values, likely indicating interference from the hydrogel (Figure 1H). In order to preserve accuracy of imaging, the array volume was restricted to 1 μl for the remainder of this work (Figure 1G). These volumes resulted in alginate spots with diameter and height of 1600 and 300 μm , respectively (Figure 1I).

Next, we determined the range of cell density over which the LI-COR Odyssey retains accuracy in quantification. Cell number should not be so high as to saturate the signal, but not so low that the signal is below the detection limit. hESCs were encapsulated at a density of 1, 3, and 5×10^6 cells ml^{-1} , stained with DRAQ5 and quantified using the LI-COR Odyssey and Image Studio software. As shown in Figure 1J, the MFI values increased by a factor of 2.8 ± 0.9 and 4.6 ± 1.6 , as seeding density was increased by a factor of 3 and 5, respectively. However, to ensure enough cells for robust protein analysis, seeding densities of 3 and 5×10^6 cells ml^{-1} were used for the remainder of this study.

3.3. Quantification of hESC Viability, Growth, and Proliferation

In our previous reports, we have shown that substrate properties can strongly modulate pancreatic differentiation of ESCs^[20–22,45]; our current objective is to develop a comprehensive platform to quantify the sensitivity of hESCs to combinatorial perturbation of substrate properties and culture configurations. In this work, culture configuration refers to encapsulating hESCs in the array starting as single cells (SC) or as preformed aggregates (Agg) formed using stirred suspension. Figure S1, Supporting Information, shows a schematic of the experimental plan. Undifferentiated (UD) hESCs were encapsulated in the array as single cells (seeding density of 3 (SC3) or 5×10^6 cells ml^{-1} (SC5)) or preformed UD aggregates, using 20–500 mM BaCl_2 to cross-link the alginate (Figure S1A, Supporting Information). Encapsulated single cells were propagated for 6 days, at which point they started forming small colonies. The encapsulated aggregates were allowed to stabilize for 2 days post encapsulation and prior to induction of differentiation, which did not

result in significant changes in aggregate size. Encapsulated hESCs were first differentiated to the definitive endoderm (DE) stage, followed by further differentiation to the pancreatic progenitor (PP) stage (Figure S1B, Supporting Information). Throughout the differentiation protocol, cell viability and proteins expression was analyzed directly on the array (Figure S1C, Supporting Information). Figure 2A illustrates cell viability by LIVE/DEAD staining performed at the end of the DE and PP

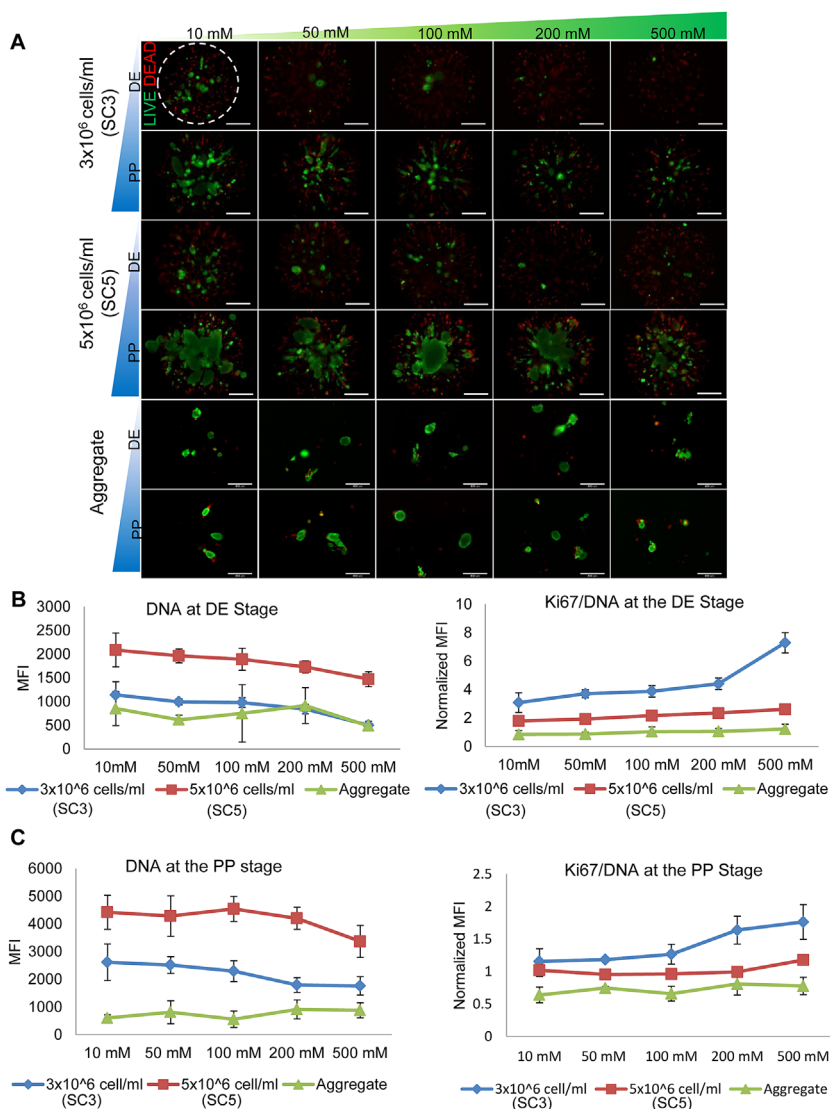


Figure 2. hESC viability and cell proliferation in response to alginate crosslinking and culture configuration. A) LIVE/DEAD assay after the DE and PP stage for encapsulated single cells, at 3 and 5×10^6 cells ml^{-1} , and aggregates, indicating cell viability in response to increasing crosslinking. Scale bar is 450 μm . B) Quantification of DNA and Ki67 protein expression after DE differentiation for single cells encapsulated at 3 or 5×10^6 cells ml^{-1} and preformed aggregates; encapsulated using 10, 50, 100, 200, and 500 mM BaCl_2 . C) Quantification of DNA and Ki67 protein expression after PP stage differentiation for single cells encapsulated at 3 or 5×10^6 cells ml^{-1} and preformed aggregates; encapsulated using 10, 50, 100, 200, and 500 mM BaCl_2 . Ki67 expression of each array spot was normalized the cellular DNA content within the array spot. Each crosslinking and culture configuration condition represents the average of $n = 5$ array spots.

stages, for each culture configuration, with simultaneous variation in the alginate substrate properties. Cell growth and proliferation was quantified by staining for DNA and Ki67 for each of the tested conditions, at both the DE and PP stages. DNA and Ki67 staining was done using LICORs near-infrared fluorophores, and quantified using the LICOR Odyssey scanner. Figure 2B and C compares cell growth, determined by the amount of total DNA present, and cell proliferation by Ki67 staining, at the DE and PP stage, for each configuration and crosslinking combination.

Both SC3 and SC5 conditions showed viable cell colonies after DE differentiation when encapsulated in 10 mM BALg, however, the number and size of viable colonies decreased as alginate crosslinking was increased. DNA quantification showed an increase in MFI with an increase in cell seeding density from 3 to 5×10^6 cells ml^{-1} (Figure 2B). For both the conditions, though, an increase in crosslinking concentration resulted in a 56 and 26% decrease in the overall DNA content for SC3 and SC5 respectively, as observed in LIVE/DEAD stain as well. Analysis of cell proliferation after DE differentiation by Ki67 staining showed that the SC3 configuration possess higher proliferative potential, compared to SC5, irrespective of substrate condition. At both seeding densities, the Ki67 expression increased slightly (45% increase for SC5) as stiffness was increased, with the exception of the SC3 configuration in the 500 mM BALg spots, which showed a sharp increase in expression (136% increase). Subsequent analysis of the PP stage showed an increase in DNA content over DE stage, for SC3 and SC5, as a consequence of proliferation. The overall trends in DNA content, however, were similar to that observed at the DE stage, showing a 32 and 23% decrease in overall DNA content for SC3 and SC5, respectively (Figure 2C). Ki67 expression at the PP stage for both single cell configurations decreased as compared to the DE stage, indicating that the cells become less proliferative with differentiation. However, a percent change of 23 and 26% for SC3 and SC5, respectively, was observed, indicating proliferation was sensitive to changes in cation concentration.

Encapsulation of preformed aggregates, in contrast to single cells, showed good viability after the DE and PP stage for each BALg condition. However, the aggregate size was fairly insensitive to the substrate properties and maintained similar sized colonies and similar DNA content throughout. Further, the aggregates did not grow appreciably over time, when differentiated from the DE to PP stage, which also contrasts with the behavior of encapsulated single cells. The Ki67 expression was lower than both single cell configurations, and insensitive to alginate stiffness. Hence, the DNA content remained similar between the DE and PP stage. Additionally, at the PP stage the aggregate configuration showed little to no change in Ki67 expression as substrate stiffness increased, similar to what was observed at the DE stage.

While cell growth was low when encapsulating hESC as aggregates, cell death was also minimal, as judged by the relative absence of red DEAD stains. Single cell encapsulation, on the other hand, resulted in significant cell death, both immediately after encapsulation as well as over propagation and differentiation. Overall these results indicate that while encapsulation of single cells showed higher expansion potential for surviving cells compared to preformed aggregates, they are more prone to cell death under encapsulation.

3.3.1. Statistical Modeling

For a more comprehensive analysis of the effect of substrate properties on hESC proliferation, we performed a regression analysis on the imaged dataset. The cation concentration was chosen as the independent variable, and the proliferation marker as the response variable. In the regression equation, non-linear dependence on the cation concentration is modeled in the form of higher order polynomial relationships (up to third order), but each such non-linear term is linear in the regression coefficients. Regression coefficients denote the strength of the contribution of the corresponding regression term to the marker level (see Section 2.7 for more details). In addition to these regression coefficients, p values of the F statistic are calculated and these denote the statistical significance of including the particular regression term in the overall equation. Data from Figure 2B and C was used to train the regression model (see Equation (1.1)).

As a first step, regression analysis was performed for each culture configuration separately. Due to experimental variability, it is necessary to check for robustness of the regression estimates. Therefore, regression analysis was repeated on multiple datasets (chosen from data for the same culture configuration and response marker) obtained by resampling of the original experimental “repeats” using a bootstrapping with replacement algorithm (see Section 2 for further details).^[46] At the end of the analysis, the distributions of regression coefficients and p values of each term in the regression equation (over bootstrapped datasets) were collected and used for comparison. From this analysis, the sensitivity of proliferation to cation concentration was determined at both the DE and PP stage, and evaluated for each culture configuration. Figure S3, Supporting Information, shows the regression coefficients for the proliferation marker Ki67. Only those bootstrap samples for which the R squared values ranged from 0.5 to 0.95 are shown (the number of such samples ranged from 50 to 95% of 1000 bootstrap samples). The x -axis includes the intercept, first order, second order, and third order terms for the DE (Figure S3A, Supporting Information) and PP stage (Figure S3B, supporting Information) for each configuration. Note that the terms for each order are multiplied by an average concentration ($C_0 = 172$ mM) of the right order so that they are in the same units and are comparable. Overall, it is found that coefficients for most terms are close to zero except for the SC3 configuration at the DE stage (p -value < 0.05). This indicates that the cation concentration, and hence, the substrate stiffness, most strongly affects the proliferation of encapsulated single cells, in particular at low seeding density. Here, the first order and second order terms are more important than the third order. This sensitivity is also apparent in the experimental data where SC3 was seen to have enhanced proliferation with increased crosslinking.

3.4. Pancreatic Differentiation of hESCs in the Alginate Array

We next evaluated how substrate conditions and culture configuration influences hESC differentiation. We have previously reported that increasing substrate stiffness enhances DE differentiation, and suppresses PP differentiation in bulk alginate capsules, formed by drop-wise addition of alginate into a cation solution.^[21]

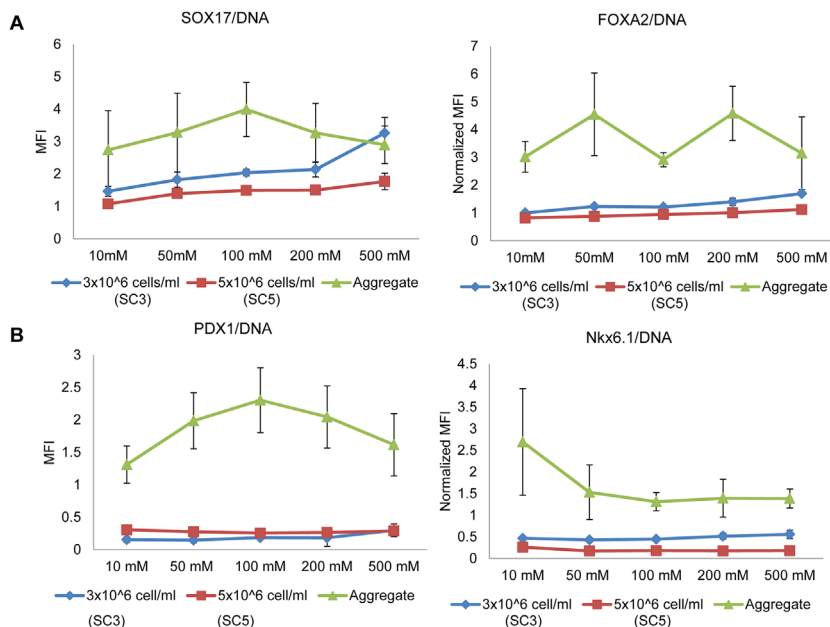


Figure 3. Analysis of DE and PP stage differentiation as alginate crosslinking and culture configuration is varied. A) Quantification SOX17 and FOXA2 protein expression after DE differentiation for single cells encapsulated at 3×10^6 cells ml^{-1} and preformed aggregates; encapsulated using 10, 50, 100, 200, and 500 mM BaCl_2 . B) Quantification PDX1 and Nkx6.1 protein expression after PP stage differentiation for single cells encapsulated at 3 or 5×10^6 cells ml^{-1} and preformed aggregates; encapsulated using 10, 50, 100, 200, and 500 mM BaCl_2 . Protein expression of each array spot was normalized the cellular DNA content within the array spot. Each crosslinking and culture configuration condition represents the average of $n = 5$ array spots.

Encapsulated hESCs were first induced to the DE stage (Figure S1B, Supporting Information), and differentiation was evaluated by SOX17 and FOXA2 protein immunostaining. These are key protein markers typically used to identify successfully DE stage differentiation^[10–13] Figure 3A presents the protein expression levels quantified using the LICOR Odyssey platform, and normalized to DNA for cell differentiated to the DE stage. Control culture of undifferentiated cells stained for SOX17 and FOXA2 showed minimal expression prior to DE inductions (Figure S2A, Supporting Information). Overall, both SOX17 and FOXA2 were observed to have a similar response to the induced physical perturbations. SC5 showed a slight increase in SOX17/DNA (≈ 1 – 1.7 , ≈ 4 – 5.1 when normalized to UD, Figure S2B, Supporting Information) and FOXA2/DNA (≈ 0.8 – 1.1 , ≈ 2.3 – 3.3 when normalized to UD, Figure S2B, Supporting Information) as substrate stiffness was increased. The same trend was observed for SC3, however, the expression of SOX17 and FOXA2 was higher than SC5 at all conditions. Interestingly, cells encapsulated as preformed aggregates showed considerably higher expression of SOX17/DNA and FOXA2/DNA, as compared to single cells. However, the aggregates showed an increase in SOX17/DNA expression as stiffness increased up to the 100 mM BALg condition, and then began to decrease as the stiffness was further increased. No obvious trend was observed in FOXA2/DNA expression with changes in stiffness.

Having confirmed germ layer commitment, we next analyzed pancreatic differentiation by quantifying the expression levels of PDX1 and Nkx6.1 proteins. Both PDX1 and Nkx6.1 are vital markers of the progenitor population required for downstream β

cell commitment, and are extensively used to characterize the pancreatic progenitor stage.^[10–13] As illustrated in Figure 3B, both SC3 and SC5 had comparable levels of PDX1 and Nkx6.1 expression levels, with PDX1 being only slightly higher in SC5 and Nkx6.1 slightly higher in SC3 conditions. However, pancreatic differentiation of single cells was largely insensitive to changes in substrate properties. In contrast to single cells, the encapsulated aggregates displayed a much stronger expression of pancreatic markers, with high sensitivity to substrate conditions. PDX1 expression increased as stiffness was increased up to the 100 mM BALg condition, and then decreased as stiffness was further increased. The nature of Nkx6.1 expression was slightly different; while PDX1 peaked around 100 mM concentration, NKX6.1 expression was highest at 10 mM concentration and dropped beyond that with increasing crosslinking. Taken together, these results indicate that differentiation is sensitive to both culture configuration and substrate properties during each stage of pancreatic differentiation.

3.4.1. Statistical Modeling

We next performed a statistical analysis to quantify the sensitivity of pancreatic differentiation to modulation of substrate properties. As before, the cation concentration was chosen as the independent variable, but now the response variables were the differentiation markers: SOX17 and FOXA2 protein at the DE stage, and PDX1 and Nkx6.1 protein at the PP stage. Figure 4 shows the regression coefficients for the differentiation markers at the DE and PP stages. As before, only those bootstrap samples for which the R squared values ranged from 0.5 to 0.95 are shown. Most samples had a higher R squared value. For example, for SOX17 in the aggregate configuration, 75% of Bootstrap samples had R squared between 0.5 and 0.95 and out of those 68% samples had R squared higher than 0.8 (Figure S4, Supporting Information). For the DE markers SOX17 (Figure 4A) and FOXA2 (Figure 4B), the influence of substrate properties is most pronounced in the aggregate configuration. The p values over the bootstrap samples are in a wider range ($0.01 < p\text{-value} < 0.1$). However, the median p values for the non-zero first and second order coefficients for SOX17, PDX1, and NKX6.1 are still below 0.05 (Table S1, Supporting Information). Similar observations can be made for the PP stage markers PDX1 (Figure 4C) and Nkx6.1 (Figure 4D). There is a minor effect of concentration in the SC3 configuration at the DE stage.

3.5. Statistical Analysis to Identify Best Predictors of Proliferation and Differentiation

The above analysis shows a somewhat disparate effect of substrate properties on proliferation and differentiation. While

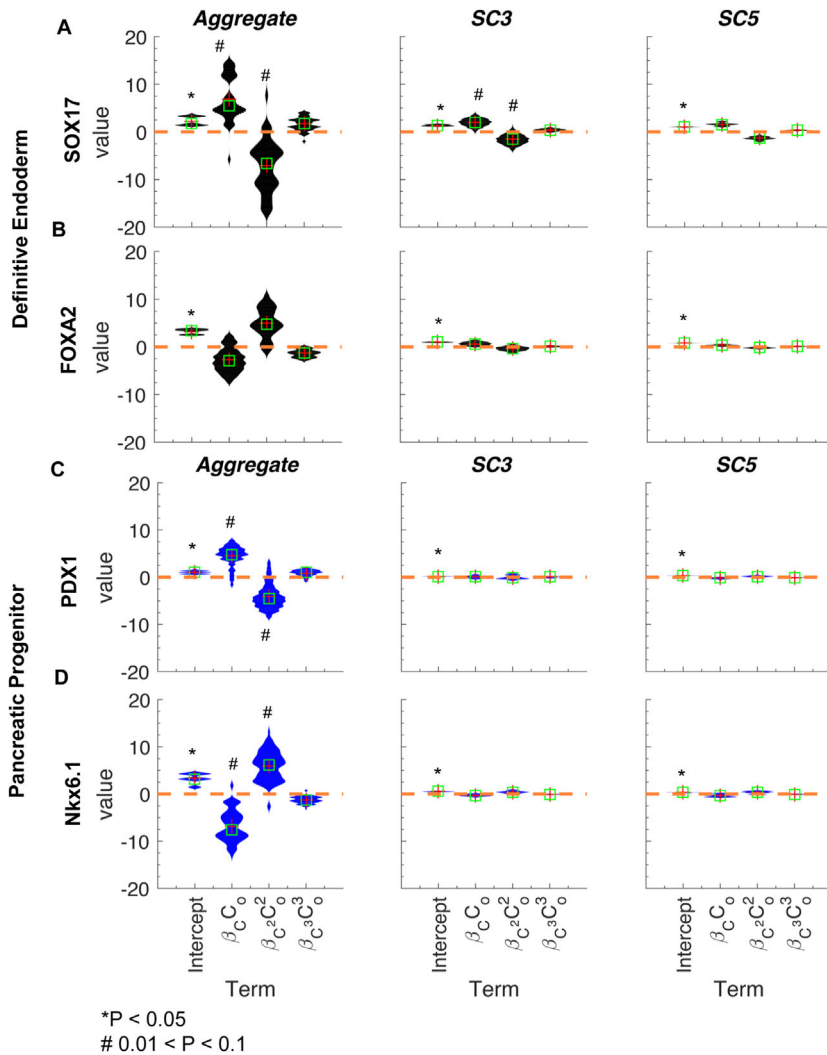


Figure 4. Significance of cation concentration in determining differentiation for each culture configuration. A and B) DE stage and (C and D) PP stage. The mean and median of the distributions in the violin plot are shown as red crosses and green squares. The p values of the F -statistic are given for the significant terms. * $p < 0.05$ and # $0.01 < p < 0.1$.

cation concentration most significantly affected the proliferation of SC3 cells, for differentiation the aggregates cultures were most sensitive to substrate properties. Thus in order to resolve the combined effect of multiple parameters (substrate properties and culture configuration) on proliferation and differentiation, a multiple regression with two independent variables was performed (Equation (1.2)). Cation concentration was chosen as a continuous variable as done in Figures S3 and S4, Supporting Information. Culture configuration being a categorical variable was encoded as follows: aggregates as “config 1”, SC3 as “config 2” and SC5 as “config 3”. During regression, a simple coding scheme was used with “config 1” as the reference level with respect to which the regression coefficients were calculated. Therefore, the regression model measures the influence of deviation of configs 2 and 3, from this reference level. In the reduced form, the model equation contains third order polynomials to describe the dependence on cation

concentration (substrate effect), linear terms for culture configurations and bi-linear terms for interaction between cation concentration and culture configuration. To compare the relative importance of configuration vs. cation concentration, the p values of the regression terms will be used. The violin plots in Figure 5 show a distribution of coefficients of each regression term for the proliferation and differentiation markers, each term brought to the same units. Figure 5A shows the coefficients for the proliferation marker Ki67 at DE and PP stage. Overall, the configuration terms are found to be most important (Intercept and configs 2 and 3) at both stages. Additionally, the interaction of config 2 and concentration shows a secondary importance at the DE (also seen from Figure 3). This term was less significant at the PP stage. Overall, these results also indicate that the contributions of each term to the proliferation marker are reduced after the DE stage.

For the differentiation markers SOX17 and FOXA2 at the DE stage, and PDX1 and Nkx6.1 at the PP stage (Figure 5B and C), the configuration terms were again important (p -value < 0.05), while the concentration terms showed a range of significance values ($0.01 < p$ -value < 0.1). The interaction between config 2 and concentration was still seen for SOX17 in a number of regression models, but this interaction was lost for other differentiation markers. Overall, this indicates that culture configuration is the stronger determinant of the average expression of the proliferation and differentiation markers while, cation concentration (and hence stiffness) fine-tunes the expression around the average levels.

4. Discussion

The objective of this study is to quantitatively evaluate the effect of combinatorial perturbations of cell microenvironment on the pancreatic differentiation of hESCs, conducted in a 3D configuration. The implementation of an alginate-based 3D microarray platform allowed simultaneous variation of both hydrogel crosslinking, as well as culture configuration (in this study, single cells or preformed aggregates). Translation of hPSCs to the clinic for regenerative cell therapy will require its large scale propagation along with functional differentiation. In addition, encapsulation in a retrievable device is a necessity in current clinical trials, in particular for diabetes therapy.^[47] Hence, in our 3D alginate array platform we evaluated the sensitivity of hESC proliferation and differentiation on encapsulation and substrate parameters. When simultaneously varying the cell density, cell culture configuration, and substrate stiffness, we identified that encapsulation of single cells at low density are ideal for cell

varying stiffness and culture configuration. Reproduction of the same stiffness range in the current array platform required higher Ba^{2+} concentrations as compared to the alginate capsules. For example, in capsules, crosslinking with 10 mM $BaCl_2$ results in approximately 4 kPa stiffness; while 150 mM $BaCl_2$ was necessary to achieve this same stiffness in the array. This difference in cation concentration needed to match the alginate stiffness in the two platforms' are likely due to differences in gelation kinetics: while alginate capsules are formed by external gelation, the alginate array is primarily by internal gelation. For example, we have previously reported the alginate hydrogel stiffness to be ≈ 1 kPa for a 1.0% alginate crosslinked with 48 mM $CaCO_3$ using internal gelation^[21]; while Morch et al. have shown that alginate of the same type and concentration, crosslinked with 50 mM $CaCl_2$ resulted in hydrogels of ≈ 10 kPa.^[48] Since different gelation methodologies could result in the different hydrogel stiffness, in the current study we chose to adjust the cation concentration in order to reproduce the desired stiffness range conducive to hESC growth and pancreatic differentiation.

Quantification of cell proliferation during pancreatic differentiation, followed by statistical analysis, revealed a significant drop in proliferation from DE to PP stage, across all the tested conditions. This is expected, since as hPSCs undergo differentiation and approach maturation, their proliferative potential is known to decrease.^[49] Comparison across encapsulation configurations indicates that lower seeding density enhances cell proliferation, for all alginate crosslinking conditions and at all stages of differentiation. Similar behavior has been reported in adherent cultures of hPSCs by Wu et al., where hPSC proliferation was found to decrease with increasing cell density.^[50] Similarly, while not in hPSCs, Stephan et al. showed that Ki67 expression was decreased in adult human intervertebral disc cells encapsulated in alginate, as seeding density was increased.^[51] Thus, DNA concentration and Ki67 expression typically exhibit an inverse correlation, which is also observed here in the trends seen for SC3 and SC5 configurations. Interestingly, however, this was not obvious in the aggregates encapsulation, which remained unchanged both in DNA and proliferation, for all stiffness conditions. Thus it is possible that pre-aggregation of the hESCs prior to encapsulation, resulted in locally minimal cell spreading, which in turn limited the proliferative capacity within the hydrogel.

However, comparison across the tested conditions showed distinct differences in sensitivity to substrate conditions. Proliferation was largely insensitive to substrate conditions, except under SC3 condition early on during differentiation (DE). The SC5 and aggregate condition had little to no sensitivity to substrate condition. This indicates that the influence of substrate properties on proliferation may be significant in the absence of high cell–cell contact. Increasing substrate stiffness increased the proliferation of SC3 cells. In addition, there was a decrease in DNA content with increasing stiffness, likely due to the hydrogel physically inhibiting cell expansion. Similar results have been seen in alginate encapsulated breast cancer cells,^[52] neural stem cells,^[53] and hESC-derived pancreatic cells.^[22]

Interestingly, the effect of substrate conditions on differentiation quite contrasted with that on proliferation. While cell

proliferation was higher in single cells, their differentiation (expression levels of DE and PP markers) was overall lower than aggregates. Single cell differentiation was also relatively insensitive to substrate conditions. In contrast, the aggregate configuration exhibited a stronger differentiation, as well as higher sensitivity to substrate conditions. This suggests that formation of tight cell-cell contacts from pre-aggregation prior to encapsulation may be promoting differentiation. This is supported by the report by Toyoda et al. showing that aggregation of human embryonic stem cells strongly enhances pancreatic bud differentiation.^[24]

Comparing the magnitudes of marker expressions, it was observed that both Sox17 and PDX1 expression peaked around 100 mM condition, while NKX6.1 decreased somewhat with increasing crosslinking concentration, the highest being at the low concentration of 10 mM $BaCl_2$. While PDX1 expression is a robust pancreatic progenitor indicator, the delineation between endocrine and exocrine cells during beta cell development is controlled in part by the expression of Nkx6.1 and Ptf1a.^[54] High expression of Nkx6.1 results in the repression of Ptf1a, leading to endocrine commitment. Previously, for alginate encapsulation of hESCs, we saw an increase in Ptf1a expression as alginate stiffness was increased.^[22] In this study, the decrease in Nkx6.1 expression could indicate loss of endocrine commitment and a potential shift to the exocrine pancreas as stiffness is increased. This is further supported by the decrease in PDX1 expression after the 100 mM conditions, as PDX1 expression has been shown to decrease as the exocrine pancreas develops.^[60] Hence possibly a lower crosslinking concentration (10–100 mM $BaCl_2$) of aggregate cultures will be better suited for pancreatic differentiation under alginate encapsulation.

Abbreviations

AFM, atomic force microscopy; BA/g, barium alginate; DE, definitive endoderm; hESC, human embryonic stem cell; PP, pancreatic progenitor; SC3, single cell encapsulated at 3×10^6 cells ml^{-1} ; SC5, single cells encapsulated at 5×10^6 cells ml^{-1} ; UD, undifferentiated.

Supporting Information

Supporting Information is available from the Wiley Online Library or from the author.

Acknowledgements

The authors acknowledge the Center for Complex Engineered Multifunctional Materials (CCEMM), Swanson School of Engineering for providing partial financial support for this research. IB also acknowledges support from NSF awards #1547618 and #1455800. PNK also acknowledges the Edward R. Weidlein Chair Professorship funds for partial financial support of this research.

Conflict of Interest

The authors declare no financial or commercial conflict of interest.

Keywords

3D, alginate, array, high-throughput, pluripotent stem cells

Received: July 26, 2017

Revised: December 9, 2017

Published online: January 25, 2018

- [1] R. S. Thies, C. E. Murry, *Development* **2015**, *142*, 3077.
- [2] S. Kadota, L. Pabon, H. Reinecke, C. E. Murry, *Stem Cell Rep.* **2017**, *8*, 278.
- [3] H. Kempf, C. Kropp, R. Olmer, U. Martin, R. Zweigerdt, *Nat. Protoc.* **2015**, *10*, 1345.
- [4] X. Lian, J. Zhang, S. M. Azarin, K. Zhu, L. B. Hazeltine, X. Bao, C. Hsiao, T. J. Kamp, S. P. Palecek, *Nat. Protoc.* **2013**, *8*, 162.
- [5] C. R. Nicholas, J. Chen, Y. Tang, D. G. Southwell, N. Chalmers, D. Vogt, C. M. Arnold, Y. J. Chen, E. G. Stanley, A. G. Elefanty, Y. Sasai, A. Alvarez-Buylla, J. L. Rubenstein, A. R. Kriegstein, *Cell Stem Cell* **2013**, *12*, 573.
- [6] D. Shimojo, K. Onodera, Y. Doi-Torii, Y. Ishihara, C. Hattori, Y. Miwa, S. Tanaka, R. Okada, M. Ohyama, M. Shoji, A. Nakanishi, M. Doyo, H. Okano, Y. Okada, *Mol. Brain* **2015**, *8*, 79.
- [7] T. Touboul, S. Chen, C. C. To, S. Mora-Castilla, K. Sabatini, R. H. Tukey, L. C. Laurent, *J. Hepatol.* **2016**, *64*, 1315.
- [8] N. R. Hannan, C. P. Segeritz, T. Touboul, L. Vallier, *Nat. Protoc.* **2013**, *8*, 430.
- [9] M. F. Leong, H. F. Lu, T. C. Lim, K. Narayanan, S. Gao, L. Y. Wang, R. P. Toh, H. Funke, M. H. Abdul Samad, A. C. Wan, J. Y. Ying, *Tissue Eng. Part C* **2016**, *22*, 884.
- [10] F. W. Pagliuca, J. R. Millman, M. Gurtler, M. Segel, A. Van Dervort, J. H. Ryu, Q. P. Peterson, D. Greiner, D. A. Melton, *Cell* **2014**, *159*, 428.
- [11] A. Reznia, J. E. Bruin, P. Arora, A. Rubin, I. Batushansky, A. Asadi, S. O'Dwyer, N. Quiskamp, M. Mojibian, T. Albrecht, Y. H. Yang, J. D. Johnson, T. J. Kieffer, *Nat. Biotechnol.* **2014**, *32*, 1121.
- [12] M. Jaramillo, S. Mathew, H. Mamiya, S. K. Goh, I. Banerjee, *Tissue Eng. Part A* **2015**, *21*, 14.
- [13] T. C. Schulz, H. Y. Young, A. D. Agulnick, M. J. Babin, E. E. Baetge, A. G. Bang, A. Bhoumik, I. Cepa, R. M. Cesario, C. Haakmeester, K. Kadoya, J. R. Kelly, J. Kerr, L. A. Martinson, A. B. McLean, M. A. Moorman, J. K. Payne, M. Richardson, K. G. Ross, E. S. Sherrer, X. Song, A. Z. Wilson, E. P. Brandon, C. E. Green, E. J. Kroon, O. G. Kelly, K. A. D'Amour, A. J. Robins, *PLoS ONE* **2012**, *7*, e37004.
- [14] D. Dufrane, R. M. Goebels, A. Saliez, Y. Guiot, P. Gianello, *Transplantation* **2006**, *81*, 1345.
- [15] D. Jacobs-Tulleers-Thevissen, M. Chintinne, Z. Ling, P. Gillard, L. Schoonjans, G. Delvaux, B. L. Strand, F. Gorus, B. Keymeulen, D. Pipeleers, B. C. T. Consortium, *Diabetologia* **2013**, *56*, 1605.
- [16] N. Li, G. Sun, S. Wang, Y. Wang, Z. Xiu, D. Sun, X. Guo, Y. Zhang, X. Ma, *Biotechnol. Appl. Biochem.* **2016**, *64*, 400.
- [17] T. Richardson, P. N. Kumta, I. Banerjee, *Tissue Eng. Part A* **2014**, *20*, 3198.
- [18] M. J. Jenkins, S. S. Farid, *Biotechnol. J.* **2015**, *10*, 83.
- [19] A. J. Engler, S. Sen, H. L. Sweeney, D. E. Discher, *Cell* **2006**, *126*, 677.
- [20] M. Jaramillo, S. S. Singh, S. Velankar, P. N. Kumta, I. Banerjee, *J. Tissue Eng. Regen. Med.* **2015**, *9*, 1.
- [21] J. Candiello, S. S. Singh, K. Task, P. N. Kumta, I. Banerjee, *J. Biol. Eng.* **2013**, *7*, 9.
- [22] T. Richardson, S. Barner, J. Candiello, P. N. Kumta, I. Banerjee, *Acta Biomater.* **2016**, *35*, 153.
- [23] L. H. Lee, R. Peerani, M. Ungrin, C. Joshi, E. Kumacheva, P. Zandstra, *Stem Cell Res.* **2009**, *2*, 155.
- [24] T. Toyoda, S. I. Mae, H. Tanaka, Y. Kondo, M. Funato, Y. Hosokawa, T. Sudo, Y. Kawaguchi, K. Osafune, *Stem Cell Res.* **2015**, *14*, 185.
- [25] J. L. Wilson, T. C. McDevitt, *Biotechnol. Bioeng.* **2013**, *110*, 667.
- [26] Y. Lei, D. V. Schaffer, *Proc. Natl. Acad. Sci. USA* **2013**, *110*, E5039.
- [27] V. C. Chen, S. M. Couture, J. Ye, Z. Lin, G. Hua, H. I. Huang, J. Wu, D. Hsu, M. K. Carpenter, L. A. Couture, *Stem Cell Res.* **2012**, *8*, 388.
- [28] J. D. Mih, A. S. Sharif, F. Liu, A. Marinkovic, M. M. Symer, D. J. Tschumperlin, *PLoS ONE* **2011**, *6*, e19929.
- [29] S. Ankam, M. Suryana, L. Y. Chan, A. A. Moe, B. K. Teo, J. B. Law, M. P. Sheetz, H. Y. Low, E. K. Yim, *Acta Biomater.* **2013**, *9*, 4535.
- [30] F. Pan, M. Zhang, G. Wu, Y. Lai, B. Greber, H. R. Scholer, L. Chi, *Biomaterials* **2013**, *34*, 8131.
- [31] C. J. Flaim, S. Chien, S. N. Bhatia, *Nat. Methods* **2005**, *2*, 119.
- [32] R. Derda, S. Musah, B. P. Orner, J. R. Klim, L. Y. Li, L. L. Kiessling, *J. Am. Chem. Soc.* **2010**, *132*, 1289.
- [33] D. Zhang, K. A. Kilian, *J. Mater. Chem. B* **2014**, *2*, 4280.
- [34] S. Gobaa, S. Hoehnel, M. Rocco, A. Negro, S. Kobel, M. P. Lutolf, *Nat. Methods* **2011**, *8*, 949.
- [35] A. Ranga, S. Gobaa, Y. Okawa, K. Mosiewicz, A. Negro, M. P. Lutolf, *Nat. Commun.* **2014**, *5*, 4324.
- [36] F. Yang, S. W. Cho, S. M. Son, S. P. Hudson, S. Bogatyrev, L. Keung, D. S. Kohane, R. Langer, D. G. Anderson, *Biomacromolecules* **2010**, *11*, 1909.
- [37] T. G. Fernandes, S. J. Kwon, S. S. Bale, M. Y. Lee, M. M. Diogo, D. S. Clark, J. M. Cabral, J. S. Dordick, *Biotechnol. Bioeng.* **2010**, *106*, 106.
- [38] M. H. Kutner, *Applied Linear Statistical Models*. McGraw-Hill Irwin, Boston **2005**.
- [39] B. Efron, R. Tibshirani, *An Introduction to the Bootstrap*. Chapman & Hall, New York **1993**.
- [40] S. Mathew, M. Jaramillo, X. Zhang, L. A. Zhang, A. Soto-Gutierrez, I. Banerjee, *BMC Syst. Biol.* **2012**, *6*, 154.
- [41] M. Y. Lee, R. A. Kumar, S. M. Sukumaran, M. G. Hogg, D. S. Clark, J. S. Dordick, *Proc. Natl. Acad. Sci. USA* **2008**, *105*, 59.
- [42] H. B. Gong, J. Kovar, G. Little, H. X. Chen, D. M. Olive, *Neoplasia* **2010**, *12*, 139-U159.
- [43] R. Tong, V. J. Coyle, L. Tang, A. M. Barger, T. M. Fan, J. J. Cheng, *Microsc. Res. Tech.* **2010**, *73*, 901.
- [44] K. M. Tichauer, K. S. Samkoe, K. J. Sexton, S. K. Hextrum, H. H. Yang, W. S. Klubben, J. R. Gunn, T. Hasan, B. W. Pogue, *Mol. Imaging Biol.* **2012**, *14*, 584.
- [45] K. Task, A. D'Amore, S. Singh, J. Candiello, M. Jaramillo, W. R. Wagner, P. Kumta, I. Banerjee, *J. R. Soc. Interface* **2014**, *11*, 20140009.
- [46] S. Mathew, M. Jaramillo, X. N. Zhang, L. A. Zhang, A. Soto-Gutierrez, I. Banerjee, *BMC Syst. Biol.* **2012**, *6*, 154.
- [47] P. G. Stock, M. S. German, *Cell Stem Cell* **2016**, *18*, 431.
- [48] Y. A. Morch, I. Donati, B. L. Strand, G. Skjak-Braek, *Biomacromolecules* **2006**, *7*, 1471.
- [49] J. C. Wu, Y. J. Fan, E. S. Tzanakakis, *Stem Cells Dev.* **2015**, *24*, 892.
- [50] J. Wu, Y. Fan, E. S. Tzanakakis, *Stem Cells Dev.* **2014**, *24*, 892.
- [51] S. Stephan, W. E. Johnson, S. Roberts, *Eur. Cell Mater.* **2011**, *22*, 97.
- [52] M. Cavo, M. Fato, L. Penuela, F. Beltrame, R. Raiteri, S. Scaglione, *Sci. Rep.* **2016**, *6*, 35367.
- [53] A. Banerjee, M. Arha, S. Choudhary, R. S. Ashton, S. R. Bhatia, D. V. Schaffer, R. S. Kane, *Biomaterials* **2009**, *30*, 4695.
- [54] A. E. Schaffer, K. K. Freude, S. B. Nelson, M. Sander, *Dev. Cell* **2010**, *18*, 1022.